Springer

Journal of Mechanical Science and Technology 23 (2009) 836~844

Journal of
Mechanical
Science and
Technology

www.springerlink.com/content/1738-494x
DOI 10.1007/s12206-008-1225-8

Performance improvement of weis-fogh type ship's propulsion mechanism using rubber type elastic wing †

Ki-Deok Ro*

School of Mechanical and Aerospace Engineering Institute of Marine Industry, Gyeonsang National University, Gyeongnam 650-160, Korea

(Manuscript Received August 14, 2008; Revised November 29, 2008; Accepted December 29, 2008)

Abstract

The performance improvement for a propulsion mechanism of Weis-Fogh type was attempted by using an elastic rubber wing. The elastic wings were made of rubber and wood with the rubber rate of 0%, 25%, and 50% in the wing area. The thrust and drag on the wing were measured for various velocity ratio V/U, opening angles of α=15° and α=30°. The average thrust coefficient and average thrust efficiency of the elastic wing were increased compared to those of the rigid wing, and the average drag coefficient was decreased; overall, by using elastic wing, the thrust, drag, and efficiency characteristics were improved. For an elastic wing with opening angle α=15° and rubber rate Rs=50% which relatively had the greatest performance improvement, thrust coefficient was increased by 30%, drag coefficient was decreased by 21%, and propulsive efficiency was increased by 17% in average compared to the rigid wing with Rs=0%.

Keywords: Hydraulic machine; Propulsion mechanism; Fluid force; Elastic wing; Rubber type; Performance improvement

1. Introduction

The Weis-Fogh mechanism[1, 2], which was discovered by the hovering flight of a small bee, is gathering attention of many scientists who study hydrodynamics, for the unique and efficient lift generation mechanism. Some scientists proposed a propulsion model that applied the principle of the mechanism, and conducted experiments on the dynamic characteristics and working test of a model ship, which showed that this propulsion mechanism worked very effectively as a new ship propulsion system[3, 4]. Also, some scientists visualized the unsteady flow fields that were created around the wings when the propulsion mechanism was being operated[5], and verified the time variation of the thrust and the drag on the wing[6].

One weakness of this propulsion mechanism is that while the maximum propulsive efficiency is high, the range of velocity ratio which generates the maximum propulsive efficiency is narrow. The velocity ratio range remains in the area under 1.0 where the thrust is relatively small. To put to practical use of this propul-

(a) Flow pattern around stopping body

(b) Flow pattern around swimming fish[7]

Fig. 1. Comparison between flow patterns around stopping body and swimming fish.

† This paper was recommended for publication in revised form by Associate Editor Yang Na

*Corresponding author. Tel.: +82 55 640 3123, Fax.: +82 55 640 3128
E-mail address: rokid@gaechuk.gsnu.ac.kr

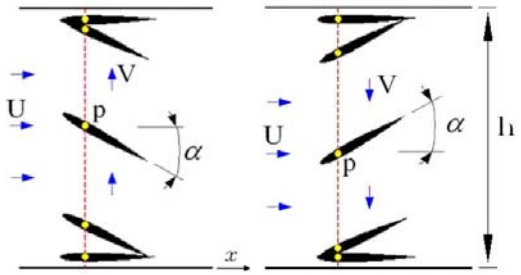

(a) Up stroke (b) Down stroke

Fig. 2. A model of propulsion mechanism.

sion mechanism, supplementing this weak point is most important. Also, to supplement this weak point, thrust needs to be improved in the wider range of velocity ratio, and drag should be decreased. In general, a drag body in the uniform flow generates a Kármán vortex in the wake region as shown in Fig. 1(a), but a swimming fish generates a vortex that is in the opposite direction of the Kármán vortex in the wake region, and it is known that the fish receives propulsive force by the jet created between the vortex rows[7], as shown in Fig. (b). By changing the rigid wing of this propulsion mechanism to a flexible flap in the trailing part to obtain the same movement as the tail of a swimming fish, the weak point mentioned above should be complemented.

In fact, the wings of a small bee and the body of a fish are elastic, and there is enough possibility that an elastic body contributes to the improvement in thrust. Therefore, in this study, the trailing part of the rigid wing will be changed into an elastic rubber wing to improve the thrust, drag, and efficiency characteristics of the propulsion mechanism

2. Experimental device and method

2.1 Model of a propulsion mechanism

Fig. 2 shows the model of the propulsion mechanism used in this experiment. The Fig. shows the upper part of the model; the wing in the water channel oscillates up and down, and the hydrodynamic forces on the wing pull it to the left (the direction toward which the ship is progressing). This model is identical to the Tsutahara and Kimura[3], and therefore a brief synopsis would be sufficient.

A wing is installed in a square channel. When the point p corresponding to the center axis of the wing is oscillated back and forth along the y axis, the wing

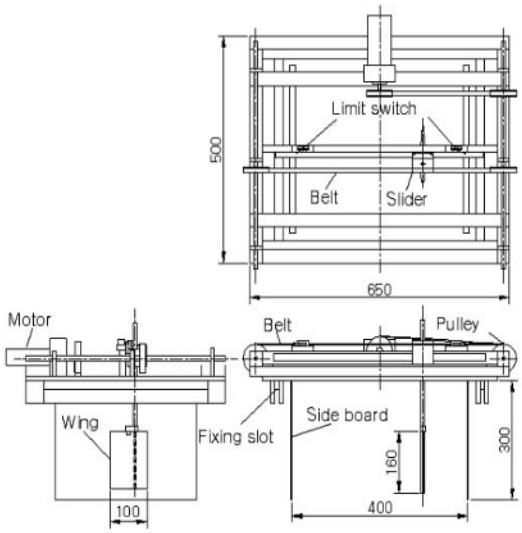

Fig. 3. Driving unit of the wing(unit: mm).

first opens at point p from the lower surface (opening stage). Then, maintaining an open angle α, the wing moves upward (translating stage), and finally rotates and closes on the upper surface (closing stage) through the reciprocal motion of point p. It then executes an opening stage at the upper surface once more, moves downward, and repeats the closing stage at the lower surface.

Originally, in the Weis-Fogh mechanism, circulation in the opposite direction is formed at each wing, as a pair of flat-plate wings open while their trailing edges touch. Through the principle of mirror image, the combination of channel walls and a single wing represents the same flow.

2.2 Measurement of the thrust and drag acting on the wing

The experiment was conducted by making a wing driving system that moves the same as the wing movement of the propulsion mechanism in Fig. 2. It was installed in the circulating water channel where uniform flow runs, and the thrust and drag on the wing were calculated by measuring the strain on the wing shaft.

Fig. 3 shows the schematic diagram of the driving unit of the wing. The main structure of the system was made with acrylic board and aluminum angle bar, and the dimensions were 500mm in length and 650mm in width to fit into the circulating water channel. In the wing driving system, the shaft was fixed

Table 1. The Spring coefficients of each elastic rubber wing.

The rate of rubber (Rs)	Rs=25%	Rs=50%
Spring coefficient (N·m/rad)	0.5291	0.4369

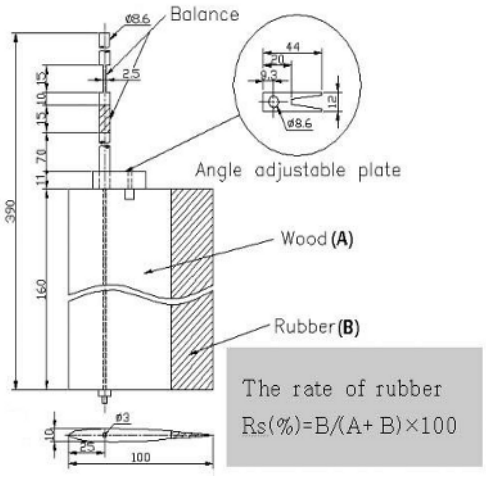

Fig. 4. Structure of the wing and shaft(unit: mm).

onto the slider and the slider was attached to one side of the belt so that when the motor (DC 30W) spun forth or backwards, the wing would move in an oscillating motion. The front and back spin of the motor was operated by a limit switch and a relay circuit installed at the ends of the slider rail; the velocity of the wing movement was controlled by adjusting the spin speed of the motor. The opening angle α is set up by attaching an angle adjustment plate on the wing shaft as shown in Fig. 4. The wing was inserted to the shaft so that when the slider moved in a translating motion, a momentum around the shaft worked toward the wing to open it, and in the closing stage, the leading edge of the wing collided with the side board, forcing it to close. The wing used in this experiment was made in the shape of NACA0010; as shown in Fig. 4, the frontal part of the wing is made of wood, and the back part is made of rubber. The wing was made in 3 different types according to the rate of rubber to whole wing area(Rs), and they are Rs=0%, 25%, 50%. The rubber part was made with just a small amount of sulfur added to the raw rubber to maintain its flexibility when the wing moved underwater. Table 1 shows the spring coefficients of each elastic wing.

The size of the wing is chord C=100mm, and its span 160mm. The shaft was penetrated at the point of 0.75C from trailing edge of the wing through a hole

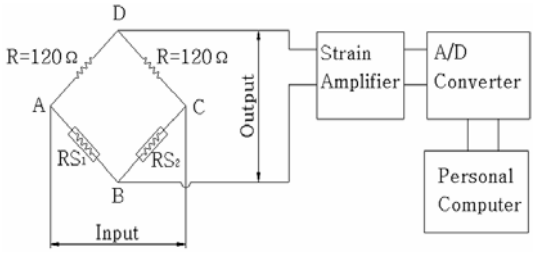

Fig. 5. Schematic diagram for the measurement of fluid force.

of 3mm in diameter. The shaft was made with an aluminum bar, 8.6mm in diameter and a stainless bar, 3mm in diameter. The balance was made by evenly cutting the top of the shaft in front, back, right and left, as shown in Fig. 4, and by attaching 4 strain gauges, thrust and drag were measured by deformation of these gauges. That is, as shown in Fig. 5, the voltage waveforms from the strain gauge outputted the value of thrust and drag by a pre-compensated coefficient on a personal computer, through a bridge circuit, strain amplifier and A/D converter in each channel(2 channels in total). The experiment fixed each wing at the opening angle α with relatively high propulsive efficiency, which was at 15° and 30°, and measured the time variation of thrust and drag by changing uniform flow U(U=0.049~0.349m/s) and wing movement velocity V(V=0.055~0.246m/s) at regular intervals. Then average thrust coefficient, average drag coefficient, and average propulsive efficiency were yielded by averaging the values in one cycle. The range of Reynolds number was $Re=7.2\times10^3$ ~3.9×10^4 when wing chord was fixed as unit length and yielded by uniform flow U.

2.3 Definition of the characteristic coefficients

Each coefficient that shows the hydrodynamic characteristics of this propulsion mechanism, that is, thrust coefficient C_T and drag coefficient C_D, are defined as follows, by wing movement velocity V.

$$C_T = \frac{T}{\frac{1}{2}\rho V^2 S} \tag{1}$$

$$C_D = \frac{D}{\frac{1}{2}\rho V^2 S} \tag{2}$$

T represents thrust, D for drag, ρ for the density of the fluid, and S for the wing area below the water surface. As defined in Fig. 5, thrust T is the component of force in the direction of the progress of the

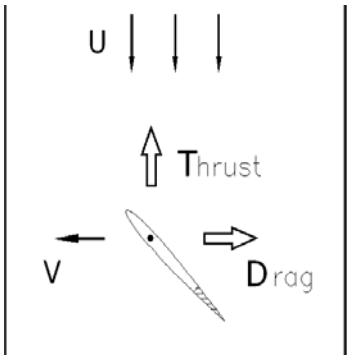

Fig. 6. Definition of thrust and drag.

ship, which is the opposite direction of uniform flow U. Drag D is the component of force in the opposite direction of the movement velocity of wing axis V. Also, the average propulsive efficiency of the mechanism $\bar{\eta}$ is the power applied to the wing, namely, the percentage of the net output generated from the wing to input, and is calculated as follows.

$$\bar{\eta} = \frac{\int_0^{T_C} C_T U dt}{\int_0^{T_C} C_D V dt} \times 100 \tag{3}$$

Here T_C represents the period of one cycle of wing movement.

2.4 Calibration of thrust and drag

The calibration of thrust and drag was executed by installing the propulsion mechanism from Fig. 3 inside an empty water channel and adding dead load in ± direction of thrust and drag in Fig. 6 at the point 1/2 of the wing span. Specifically, using the circuit in Fig. 5, voltage output that corresponded to each load was obtained by increasing 0.3N in ±0.9N range for thrust; drag was increased by 1N in the range of ±4.0N. With this data, load and voltage output relation was deduced by linear least squares approximation.

Fig. 7 shows the calibration results of thrust and drag executed on the measuring shaft in Fig. 4. As illustrated in Fig. 7, the results of the calibration show that both thrust and drag were on a straight line, and the error range of root-mean square from the experimental value and the linear relation value of thrust and drag were all under 0.01. Therefore, as in this experiment, by evenly cutting the balance of the round measuring shaft in front, back, right and left, and attaching 4 strain gauges as shown in Fig. 4, each perpendicular force can be measured conveniently.

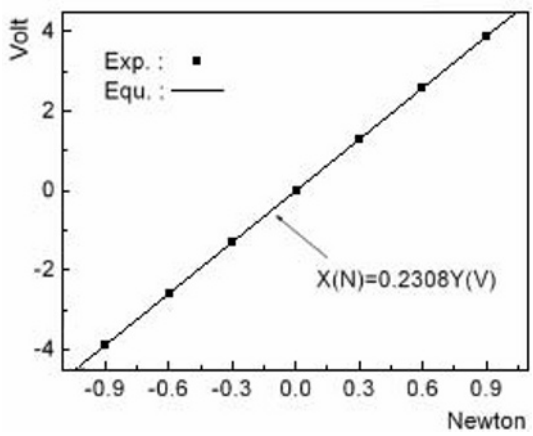

(a) Thrust

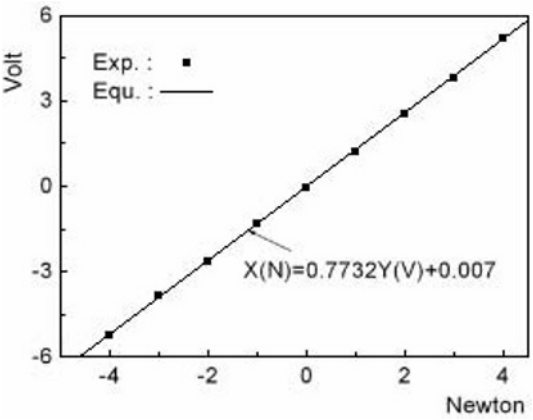

(b) Drag

Fig. 7. Calibration results of thrust and drag.

3. Results and discussion

The experiment was conducted as in the previous study[6], with a wing section of NACA0010 Type, width of water channel h=4C(C: wing chord) and the distance from the trailing edge of the wing to the wing axis fixed to r_p=0.75. Also, thrust and drag acting on the wing was measured by changing the ratio V/U, which is the moving velocity of the wing axis to uniform flow, at opening angles of α=15° and α =30, where the maximum thrust efficiency is relatively high[3, 4].

Fig. 8 shows the time variations of thrust coefficient C_T and drag coefficient C_D over 2 reciprocating movements of the wing at opening angle α=15° and velocity ratio V/U=0.91. The dotted line and solid line in the Fig. each expresses the rate of rubber to whole

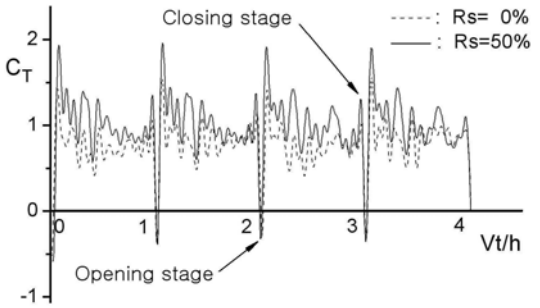

(a) Thrust coefficients

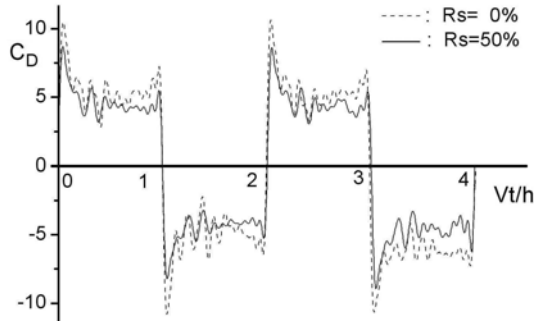

(b) Drag coefficients

Fig. 8. Time variations for thrust and drag coefficients (α=30°, V/U=0.93).

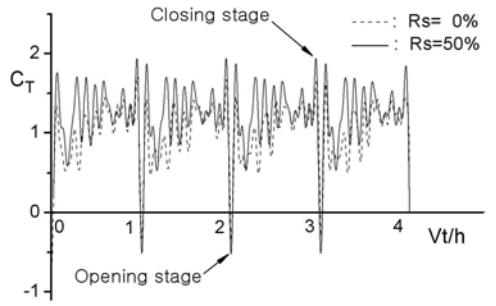

(a) Thrust coefficients

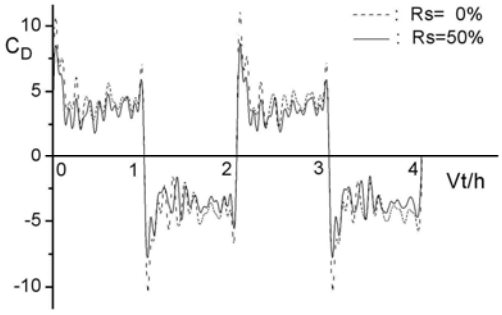

(b) Drag coefficients

Fig. 9. Time variations for thrust and drag coefficients (α=30°, V/U=0.93).

wing area Rs=0% and 50%, respectively, and the x-axis expresses the traveling distance of wing shaft normalized by the channel width; this value means the number of strokes. First, when looking at the change of thrust coefficient, the value was + through the whole stroke except for the opening stage, and regardless of the wing's reciprocating motion, thrust occurred toward the direction of the progress of the ship, which consists with the former research results[3, 4]. Also, at both Rs=0% and 50%, very big values could be seen at the early stage of each stroke. This seems to be because during the opening stage, the motion changed into translation stage, and the opening angle suddenly became stabilized, which instantly applied unsteady force to the wing. Also, in one stroke, the large fluctuations of thrust were due to the surface wave and vortex shedding occurring from the movement of the wing. When comparing Rs=0% and 50%, in one stroke, the elastic wing with Rs=50% always had larger value than the rigid wing with Rs=0%; this shows that the elastic wing contributed to the im provement in thrust. However, through the whole stroke, the overall dynamic characteristics showed a similar ten-

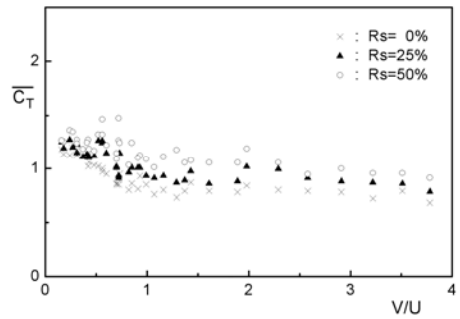

(a) Average thrust coefficients

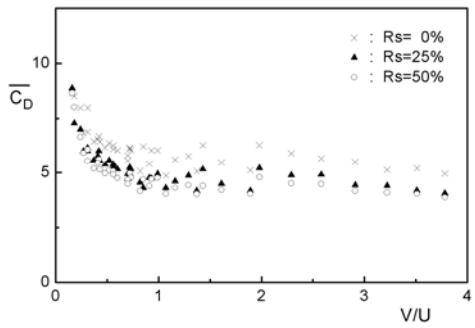

(b) Average drag coefficients

Fig. 10. Average thrust and drag coefficients with velocity ratio (α=15°).

dency for both. Next, in the change of drag coefficient C_D by time, in each stroke, the value was reversed with x-axis; this is because each stroke of the wing movement was in the opposite direction. As well as the thrust coefficient, the drag coefficient also shows big values at the beginning of a stroke in Rs=0% and 50%, and this is because of the inertia from wing reversal, like thrust coefficient. Comparing Rs=0% and 50%, in a stroke, The elastic wing always has a smaller value of drag coefficient than a flat-plate wing; the reason for this will be explained thoroughly in Fig. 10.

Fig. 9 shows the time variations of thrust coefficient C_T and drag coefficient C_D over 4 strokes of the wing at opening angle α=30° and velocity ratio V/U=0.93. When looking at the change of thrust coefficient, just as in Fig. 8(a), the value was + through the whole stroke except for the opening stage, and regardless of the wing's reciprocating motion, in one stroke, elastic wing with Rs=50% always had a larger value than the rigid wing with Rs=0%. The change of drag coefficient also was the same as Fig. 8(b); the drag coefficient showed big values at the beginning of stroke in Rs=0% and 50%. When comparing Rs=0% and 50%, in one stroke, the elastic wing always had a smaller value in drag coefficient than the rigid wing. That is, regardless of the change in the opening angle, the thrust and drag characteristics in time variation showed similar tendency. $\overline{C_T}$ and (b) time-averaged drag coefficient $\overline{C_D}$ with the velocity ratio V/U at opening angle α=15°.Each point in Fig. 10(a), (b) corresponds with the time-averaged value of 1 cycle of time variations for thrust and drag coefficients as shown in Fig. 8(a), (b) in each velocity ratio, respectively. First, when looking at the distribution of average thrust coefficient, the values were almost constant regardless of the velocity ratio. Where the rate of rubber was 25% or 50%, the values did not have much difference; but when compared with 0%, the ones with rubber had a larger value than the one with no rubber in the overall velocity ratio. When looking at the distribution of average drag coefficient, over velocity ratio of 0.5, the values were almost constant, whereas under 0.5, they increased as velocity ratio decreased. This is because under the velocity ratio of 0.5, the maximum opening angle was smaller than 15°, which led to an increase in drag. When comparing by the ratio of rubber, the average drag coefficient also had similar values with 25% and 50% of rubber, but when compared with 0%, the ones with rubber had smaller

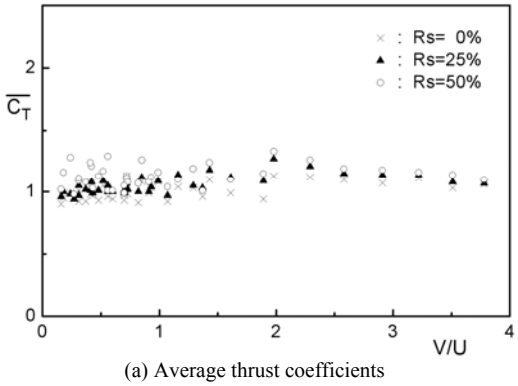

(a) Average thrust coefficients

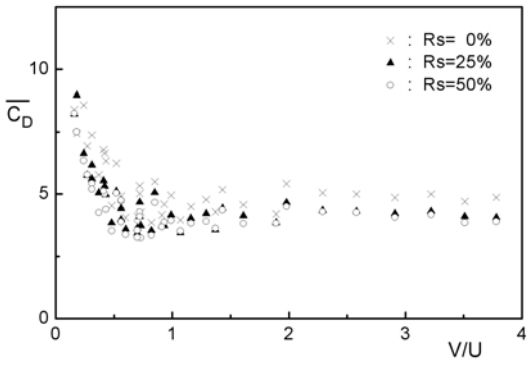

(b) Average drag coefficients

Fig. 11. Average thrust and drag coefficients with velocity ratio (α=30°).

value than the one with no rubber. This is because the elastic rubber wing is more elastic than the rigid wing; therefore, when the wing moves, by water resistance, deformation occurs in the opposite direction of the progressing direction of the wing in the trailing part, which decreases the drag on the wing.

Fig. 11 shows (a) time-averaged thrust coefficient $\overline{C_T}$ and (b) time-averaged drag coefficient $\overline{C_D}$ with the velocity ratio V/U at opening angle α=30°. First, when looking at the distribution of average thrust coefficient, just as in Fig. 10(a), the average thrust coefficient was generally bigger with an elastic wing than a rigid wing, and when comparing the elastic wings, Rs=50% with larger rubber rate had bigger thrust coefficient than Rs=15%. Also, when comparing Fig. 10(a) and Fig. 11(a), the increasing rate of elastic wings was bigger in the case of smaller opening angle of α=15° than α=30°which had a bigger opening angle. When looking at the distribution of average drag coefficient, just as in Fig. 10(b), the average drag coefficient was almost constant when the velocity ratio was over V/U=0.5. But when it was under V/U=0.5, as the

velocity ratio decreased, the average drag coefficient increased. Also, when comparing the ratio of rubber, as in Fig. 10(b), the average drag coefficient also had similar values with 25% and 50% of rubber, but when compared with 0%, the one with rubber had smaller value than the one with no rubber. For the reason of the outcomes, it is as explained in Fig. 10(b). On the other hand, when comparing Fig. 10(a),(b) and Fig. 11(a),(b), an opening angle of α=30°had a bigger average thrust coefficient in overall velocity ratio, but the average drag coefficient was smaller compared to α=15°.

Fig. 12 shows the average propulsive efficiency at opening angle (a) α=15° and (b) α=30° with the velocity ratio V/U. When looking at the distribution of average propulsive efficiency, in (a) and (b), both of the velocity ratios had a maximum value under 0.5, but where the velocity ratio was over 1.0, (b) with the bigger opening angle was little bit larger than (a) with a smaller opening angle, which is consistent with the earlier research[3-4]. Also, although there are some differences according to velocity ratio, in both (a) and (b), the one with elastic rubber had larger propulsive efficiency than the rigid wing with no rubber, and the values increased as the area of elastic rubber increased as Rs=0%, 25%, and 50%.

Table 2 shows the average increasing rates of thrust, drag coefficients and propulsive efficiency for each elastic wing as compared with the rigid wing(Rs=0%) The average increasing rates in Table 2 were obtained from the values of each average coefficient in Figs. 10, 11, and 12. They were averaged by the overall velocity ratio. However, as shown in Figs. 10, 11, and 12, the data numbers of each coefficient were different with the range of velocity ratio. Therefore, to yield the overall average increasing rate, the velocity ratio was divided by 4 equal sections, and by each section, the average increasing rate of each coefficient was obtained; then they were re-averaged by the 4 sections. In Table 2, the average thrust coefficient and propulsive efficiency of elastic wing were increased compared to those of the rigid wing, and the average drag coefficient was decreased. Therefore, in general, by using an elastic wing, the thrust, drag, and efficiency characteristics were improved. Also, when compared by the rubber rate Rs, in both opening angle α=30° and α=15°, the average increasing rate of each coefficient was bigger with Rs=50% than Rs=25%. Overall, in the case of the elastic wing with opening angle α=15° and rubber rate Rs=50% which relatively

Table 2. The average increasing rates of thrust, drag coefficients and propulsive efficiency for each elastic wing as compared with the rigid wing(Rs=0%).

α	α=15°		α=30°	
R_S	Rs=25%	Rs=50%	Rs=25%	Rs=50%
$\overline{\Delta C_T}$	15%	30%	6%	11%
$\overline{\Delta C_D}$	-17%	-21%	-14%	-16%
$\overline{\Delta \eta}$	15%	17%	17%	19%

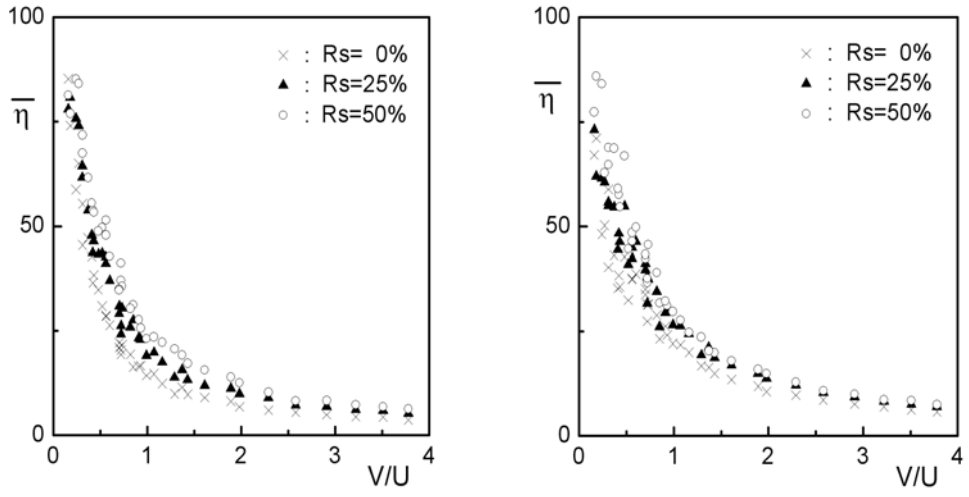

(a) α=15° (b) α=30°

Fig. 12. Average propulsive efficiency with velocity ratio.

had greatest performance improvement, the thrust coefficient was increased by 30%, drag coefficient was decreased by 21%, and propulsive efficiency was increased by 17% on average, compared to the rigid wing with Rs=0% in same condition.

4. Conclusions

This experiment was conducted in an attempt to enhance the performance of the propulsion mechanism by changing a rigid wing into an elastic rubber wing in the Weis-Fogh type ship propulsion mechanism. The elastic wing was made in 3 types: the rate of rubber to whole area was 0%, 25%, and 50%. The opening angle was fixed at α=15° and α=30°, and by changing velocity ratio V/U, thrust, drag, and propulsive efficiency were examined experimentally. The summaries of results are as follows: The average propulsive coefficient and average thrust efficiency of elastic wing were increased compared to those of the rigid wing, and the average drag coefficient was decreased; therefore overall, the thrust, drag, and efficiency characteristics improved in using the elastic wing. Also, Rs=50% that had larger rubber rate had more improvement in the opening angle of α=30° and α=15°, compared to Rs=25%. In the case of the elastic wing with opening angle α=15° and rubber rate Rs=50% which relatively had greatest performance improvement, thrust coefficient was increased by 30%, drag coefficient was decreased by 21%, and propulsive efficiency was increased by 17% in average, compared to the rigid wing with Rs=0% in same condition. And, the characteristics of time variation in thrust and drag had same tendency in both the elastic wing and the rigid wing. In addition, as in this experiment, by evenly cutting the balance of the round-profile measuring shaft in front, back, right and left and attaching 4 strain gauges, each perpendicular force can easily be divided and measured.

Acknowledgment

This work was supported by the Korea Science and Engineering Foundation (KOSEF) grant funded by the Korea government(MOST) (No.R01-2007-000-10038-0)

Nomenclature

C	:	Chord length of wing
C_T	:	Thrust coefficient
C_D	:	Drag coefficient
$\overline{C_T}$	:	Time-averaged thrust coefficient
$\overline{C_D}$	:	Time-averaged drag coefficient
D	:	Drag acting on wing
h	:	Width of water channel
p	:	Center axis of wing
R_e	:	Reynolds number
r_p	:	Distance from the trailing edge of wing to wing axis
R_S	:	Rate of rubber area to whole wing area
S	:	Wing area below water surface
T	:	Thrust acting on wing
T_C	:	Period of one cycle of wing movement
U	:	Uniform flow
V	:	Movement velocity of wing axis
α	:	Opening angle
$\overline{\Delta C_T}$	:	Average increasing rate of thrust coefficient
$\overline{\Delta C_D}$	:	Average increasing rate of drag coefficient
$\overline{\eta}$	:	Average propulsive efficiency
$\overline{\Delta \eta}$	:	Average increasing rate of propulsive efficiency
ρ	:	Density of fluid

References

[1] T. Weis-Fogh, Quick Estimates of Flight Fitness in Hovering Animals, Including Novel Mechanism for Lift Production, *J. Exp. Bio*. 59 (1973) 169-231.

[2] M. J. Lighthill, On the Weis-Fogh Mechanism of Lift Generation, *J. Fluid Mech*, 60 (1973) 1-17.

[3] M. Tsutahara and T. Kimura, An Application of the Weis-Fogh Mechanism to ship Propulsion, *J. Fluids Eng*., 109 (1987) 107-113.

[4] M. Tsutahara, T. Kimura and K. D. Ro, Ship Propulsion Using the Weis-Fogh Mechanism, *Bull. MESJ*, 17-2 (1989) 49-55.

[5] K. D. Ro, K. S. Kim and J. H. Kim, The Flow Characteristics around Airfoil Moving Reciprocally in a Channel, *Trans. KSME*, 32-7 (2008) 536-541 (in Korean).

[6] K. D. Ro, B. S. Zhu and H. K. Kang, Numerical Analysis of Unsteady Viscous Flow Through a Weis-Fogh Type Ship Propulsion Mechanism Using the Advanced Vortex Method, *J. Fluids Eng*., 128 (2006) 481-487.

[7] D. Weihs, Some Hydrodynamical Aspects of Fish Schooling, In *Swimming and Flying in Nature*, 2 (1975), Plenum Press· New York and London, 703-

718.

Ki-Deok Ro received his B.S. degree in Marine Engineering from Pukyong National University, Korea, in 1977. He then received his M.S. and Ph.D. degrees from Kobe University, Japan, in 1986 and 1989, respectively. Dr. Ro is currently a Professor at the School of Mechanical Engineering at Gyeongsang National University in Gyeongnam, Korea. He serves as an Editor of Journal of the Korean Society of Marine Engineering. Dr. Ro's research interests include fluid mechanics, CFD, and vortex method.